Quantitative and dynamic assay of single cell chemotaxis

Lee, Sung Sik ; Horvath, Peter ; Pelet, Serge ; Hegemann, Björn ; Lee, Luke P ; Peter, Matthias

Abstract: We have developed a single-cell assay platform that allows quantitative analysis of single cell chemotaxis by dynamic morphogenetic gradients, subcellular microscopic imaging and automated image analysis, and have applied these to measure cellular polarization of budding yeast. The computer-controlled microfluidic device regulates the gradient profile at any given time, and allows quantitative monitoring of cell morphology and the localization and expression of specific marker proteins during the dynamic polarization process. With this integrated experimental system, we compare the polarized signaling response of wild-type and far1-H7 mutant cells, which express a truncated Far1 protein unable to interact with Cdc24. Our results confirm that Far1 functions as an adaptor that recruits polarity establishment proteins to the site of extracellular signaling. Moreover, by changing the gradient profile and estimating the number of bound surface receptors, we quantitatively address why surprisingly small differences in pheromone concentration across yeast cells can be amplified into a robust polarity axis. This integrated single cell experimental platform thus opens the possibility to quantitatively investigate the molecular regulatory mechanism of chemotaxis in yeast, which serves as a paradigm to understand the fundamental processes involved in cancer metastasis, angiogenesis and axon generation.

DOI: https://doi.org/10.1039/c2ib00144f

Quantitative and Dynamic Assay of Single Cell Chemotaxis

Sung Sik Lee [a,b], Peter Horvath [c], Serge Pelet [a,b], Björn Hegemann [a],

Luke P. Lee *,[d], and Matthias Peter §,[a,b]

[a] Institute of Biochemistry, ETH Zurich, Zurich, CH 8093, Switzerland

[b] Competence Center for Systems Physiology and Metabolic Disease(CC-SPMD), Zurich, CH 8093, Switzerland

[c] Light Microscopy Center (LMC), Department of Biology, ETH Zurich, Zurich, CH 8093, Switzerland

[d] Berkeley Sensor & Actuator Center, Department of Bioengineering, University of California, Berkeley, CA 94720-1762, United States

Co-correspondences:

* lplee@berkeley.edu; Tel: +1-510-642-5855, Fax: +1-510-642-5835

§ matthias.peter@bc.biol.ethz.ch ; Tel: +41-44-633-6586, Fax: +41-44-633-1298

Abstract

We have developed a single-cell assay platform that allows quantitative analysis of single cell chemotaxis by dynamic morphogenetic gradients, subcellular microscopic imaging and automated image analysis, and have applied these to measure cellular polarization of budding yeast. The computer-controlled microfluidic device regulates the gradient profile at any given time, and allows quantitative monitoring of cell morphology and the localization and expression of specific marker proteins during the dynamic polarization process. With this integrated experimental system, we compare the polarized signaling response of wild-type and *far1-H7* mutant cells, which express a truncated Far1 protein unable to interact with Cdc24. Our results confirm that Far1 functions as an adaptor that recruits polarity establishment proteins to the site of extracellular signaling. Moreover, by changing the gradient profile and estimating the number of bound surface receptors, we quantitatively address why surprisingly small differences in pheromone concentration across yeast cells can be amplified into a robust polarity axis. This integrated single cell experimental platform thus opens the possibility to quantitatively investigate the molecular regulatory mechanism of chemotaxis in yeast, which serves as a paradigm to understand the fundamental processes involved in cancer metastasis, angiogenesis and axon generation.

Introduction

Cells continuously sense their extra- and intracellular environment and respond to changes by activating dynamic signaling networks. Genetic and biochemical approaches have identified numerous signaling components and have organized their activities into specific pathways. These methods generally rely on data averaged from large cell populations, but quantitative and dynamic single cell measurements are a prerequisite to deduce signaling kinetics suited to develop mathematical models that accurately describe the complex cellular responses [1-4]. For example, such single cell measurements combining microfluidic devices with quantitative live cell imaging recently revealed new insights into how the Hog1 Mitogen Activated Protein-kinase (MAPK) pathway responds to osmotic stress [5-9].

While some signals are transmitted as an all-or-none response, many cells respond to intra- or extracellular gradients. Most notably, many cell types use chemotactic gradients to deduce directional information, including repulsion and attraction signals. These cells not only manage to sense the presence of a given diffusible signal, but they also interpret the concentration and location of the source to direct their response. Morphogenetic gradients pattern many tissues during embryo development; Specific attractant and repulsion cues guide axons in the developing nervous system[10]; Neutrophils in the immune system polarize and migrate towards a pathogen[11]; Tumors induce growth of blood vessels (angiogenesis) towards various secreted growth factors[12]. However, little is known at the molecular level of how such morphogenetic signals are sensed and amplified, in part due to the lack of suitable experimental systems to investigate these complex temporal and spatial responses.

The mating response of budding yeast *S. cerevisae* emerged as a genetically tractable model system to elucidate the underlying spatial and temporal regulatory mechanism of gradient sensing pathways. Specifically, yeast cells orient their cytoskeleton along the mating pheromone α-factor gradient (Fig.1A) to promote cell fusion with a mating partner. The spatial information of the gradient is sensed by the binding of α-factor to

dedicated seven-transmembrane spanning receptors coupled intracellularly to heterotrimeric G-proteins (GPCRs). The activated G-proteins then locally trigger the MAPK cascade, and the activated MAPK mounts a cellular response culminating in the cytoskeletal orientation towards the highest concentration of pheromone and formation of a mating projection, the so-called ”shmoo”. However, to be able to deduce directional information from this α-factor gradient, the cell must also possess amplification mechanisms that allow for differentiating between extremely small differences in ligand concentration across its surface diameter of 4 - 5 μm. Key components that govern cellular polarization along pheromone gradients include the scaffold protein Far1 (Factor arrest 1), which binds to the Cdc42 (Cell division cycle 42), the exchange factor Cdc24 (Cell division cycle 24) and its activator Bem1 (Bud emergence 1). However, quantitative information on the temporal and spatial regulation of these components is needed to elucidate their mode of action and deduce mathematical models that help to explain the resulting directional response.

Despite the powerful genetic and molecular tools offered by the budding yeast system, the quantitative and dynamic analysis of this morphogenetic response pathway has been hindered by the lack of a robust experimental platform that allows quantitative live imaging with tunable and stable gradients. Conventionally, concentration gradients of α-factor are created for cells grown on agarose pads by continuously dropping α-factor solution with a given concentration through a micropipette [13, 14] (Supplementary Fig.S1). Diffusion of α-factor from this “point source” creates a gradient, and the directional response of yeast cells near the center can be monitored over time. However, because of the thickness of the opaque agar pad, the working distance of the objectives prevents high-resolution imaging of fluorescently labeled marker proteins. Moreover, it is difficult to estimate the gradient profile across the cells. Recently, microfluidic devices were developed as an alternative method to establish stable α-factor concentration gradients [15, 16]. These devices greatly improved the reproducibility of the applied gradient profiles, and also increased the resolution possible for

optical imaging. However, because gravity-driven flow or syringe pumps utilize wet-tubing, the stability of the gradients over long time frames is challenging, and the gradient profiles are difficult to regulate. In addition, automated image analysis methods are needed to quantify the cellular response, including the gradual elongation of the mating projection and the dynamic recruitment of specific marker proteins to sites of polarization by live cell imaging with fluorescent probes.

Here, we demonstrate a quantitative and dynamic assay platform to analyze single cell chemotaxis. This platform circumvents previous limitations and significantly expands the reproducibility and versatility of microfluidic gradient systems. We developed computer-controlled integrated microfluidic systems that can stably regulate the desired gradient profiles and can interface with multi-dimensional live cell microscopy instrumentation equipped with automated image analysis programs (Fig. 1B and Supplementary Fig. S2) that automatically segment and quantify the shmoo-like cell morphology, intracellular protein localization (Fig.1C) and polarization (Fig.1D). We validated this integrated experimental platform by comparing the directed response of wild-type cells, and cells expressing a mutant form of the mating scaffold Far1 (Far1-H7). Finally, by quantifying the cellular response in different gradient profile concentrations, we were able to deduce a mathematical model that may explain how differential receptor occupancy can translate the small concentration difference across the cell surface into a robust axis of polarization.

Results and Discussion

Regulation of gradient profiles by a computer-controlled microfluidic system

To develop a microfluidic platform that supports stable concentration gradients, we first reduced the dead volume of wetted tubing that was needed for operating syringe pumps or gravity-driven flows. To achieve this, we directly attached two separate feeder wells to the

device, each with a maximum volume of 300 µL, similar to the volume in a single well of a 96-well plate (Fig. 2A and Supplementary Fig. S3). Two separate feeder wells contain media with a molecule of interest at two different concentrations, which define the upper and lower limit of the gradient. Fluidic resistances comprised of a narrow serpentine channel were designed next to the reservoirs to dampen the flow fluctuations and to tune the flow rates of medium using Ohm's Law ($Q = \Delta P / R$, Q: volumetric flow rate, ΔP: pressure drop, R: fluidic resistance, *e.g*, $Q \approx 0.2$ µL / min at $\Delta P = 1.5$ psi in this device $R \approx 3.1 \times 10^{15}$ $m^5N^{-1}s^{-1}$). This set-up reduces the volume of medium, with less than 200 *µL* of media sufficient to ensure continuous flow during an overnight experiment (more than 16 hrs, $Q \approx 0.2$ µL / min at $\Delta P =$ 1.5 psi). This procedure avoids gradient instability due to stick-slip in the syringes commonly observed when using syringe pumps [17, 18]. Moreover, it circumvents the common problems associated with gravity flows in the use of long tubing and large reservoirs, such as the appearance of air bubbles in the wetted tubing solution.

Yeast cells are sensitive to high flow rates, since shear stress can trigger the MAPK pathway[19, 20] and interfere with mating signaling. To reduce flow across the cell culture chamber, we designed specific convection barriers containing two rows of zigzag-like pillar arrays (100 *µm* x 100 *µm* dimension of each pillar) separated by gaps of 7 *µm* (Fig. 1B). Since most of the medium released from the reservoirs flows through the wider channel and thus not directly to the cell culture chamber, the flow rate across the cell culture chamber is significantly reduced. Indeed, numerical simulation (COMSOL Multiphysics 4.2, COMSOL Inc.) confirmed that the flow rate in the cell culture chamber is lower compared to the wider channel above the pillar array (Fig. 2B). Taken together, this novel design avoids washing away the attached yeast cells, and significantly reduces flow disturbance in the chamber.

To precisely control the flows and create accurate and stable gradient profiles, we next introduced a computer-controlled pneumatic regulator (Fig. 2A and Supplementary Fig. S2). The regulator provides specified hydrostatic pressures (*e.g.* ΔP_H, ΔP_L: 0.25 – 10 *psi*) that

controls the volume of media introduced into the cell culture chamber from each of the two reservoirs, and thus controls the gradient profile in the cell culture chamber with a ratio of the applied pressures (e.g. $\Delta P_H / \Delta P_L$). The on-off timing of the applied pressure is triggered by the computer-derived electric signal, which controls the gradient profile at a given time (Supplementary Figure S2 and S3). To test this set-up, we visualized and quantified the gradient profiles in the cell chamber using a fluorescent dye (tetramethylrhodamine-dextran, *M.W.*= 3,000; Invitrogen). As shown in Fig. 2C and D, the gradient profile was established in less then 2 min with $\Delta P_H = \Delta P_L$ = 3 *psi*, and the established gradient profile remained stable over four hours, an essential prerequisite for monitoring kinetics of polarization across the small diameter of yeast cells (5 μm) (Fig. 2E). Importantly, the gradient profile could be tuned by controlling the ratio of the pressures (e.g. $\Delta P_H / \Delta P_L$) (Fig. 2F and 2G), which allows for studying the cellular response to precise morphogenetic gradients. Taken together, the computer-controlled microfluidic platform is able to rapidly establish a stable and accurate gradient, which can be dynamically regulated.

Automated quantification of polarized budding yeast growth in α-factor gradients

To test the microfluidic device, we imaged living yeast cells by time-lapse microscopy. The cells were immobilized in the cell culture chamber by concanavalin-A treatment, and their response was first monitored to uniform α-factor concentrations. These cells were engineered to express a mating-specific reporter, based on the *FIG1* (Factor Induced Gene 1) promoter driving the expression of quadruple-Venus fluorescent protein (p*FIG1*-qV, Note: Venus is Yellow Fluorescent Protein variant - YFP) specifically induced upon activation of the mating MAPK signalling cascade triggered by α-factor[9]. Without α-factor (0 nM), no YFP fluorescence can be detected and the budding yeast cells form buds (Supplementary Fig. S4). In contrast, in uniform α-factor concentration (200 nM), the cells express YFP and specifically arrest in the G1 phase of the cell cycle. In addition, these cells polarize their

cytoskeleton, leading to the elongated shmoo morphology (Supplementary Fig. S4). Since α-factor is uniformly distributed under these conditions and thus binds receptors over the entire cell surface with the same probability, the direction of polarized growth is random and determined by α-factor-independent polarity cues. Nevertheless, these results imply that the yeast cells are able to grow in our microfluidic cell culture chamber for extended periods of time, and are capable of pheromone response.

We next determined whether yeast cells respond directionally in physiologically-relevant morphogenetic gradient conditions. Importantly, in 0- 200 nM α-factor gradients wild-type (WT) cells polarized towards higher concentrations (Fig. 3A and Supplementary Movie S1). The actual gradient in the cell chamber was visualized by tetramethylrhodamine-dextran, (*M.W.* = 3000), shown in blue in Fig. 3A).

To quantify this oriented polarization response, we developed a Matlab-based image analysis program that automatically tracks the cellular morphology over time, and calculates the growth axis angle relative to the direction of the α-factor gradient. To segment the border of shmoo-like cells, bright field images were used to efficiently define the cellular outline using active contours[21]. The active contours extend with the intensity gradient vector flow[22] framework and find the outline of the cell (e.g. from red to blue line in Fig.3B). Note that in this procedure the intensity gradient is deduced from the bright field image and is not based on the fluorescent gradient profile. The detailed segmentation method is described in the experimental section. After segmentation, the gradual cell elongation and α-factor signaling to the downstream pathway could be quantified using the circularity index (*circularity* = 4π (*area* / *perimeter* ^{2}) and the total intensity of the mating-specific *FIG1*-qV fluorescent reporter, respectively (Fig. 3A and C). Importantly, using this method, the accuracy and dynamics of oriented individual cell polarization could be automatically quantified (Fig. 3C and D). The experimental data demonstrate that in the physiological range of the applied α-factor gradient most wild-type cells elongate and direct new surface growth towards the highest

concentration of pheromone. Interestingly, while most cells appear to polarize along the pheromone gradient angle from the beginning, others (arrow in Fig. 3A) adjust their angle of polarized growth during the process (Fig. 3A), implying that dynamic mechanisms must exist that allow for correction of the polarization axis.

To validate this integrated microfluidic gradient platform, we next investigated the role of Far1, postulated to function as a scaffold to sense the directionality of the pheromone gradient. Far1 is recruited to the site of engaged α-factor receptors by directly interacting with the activated heterotrimeric G-protein. In turn, Far1 binds and activates the guanine nucleotide exchange factor Cdc24, leading to local activation of the Rho-type GTPase Cdc42, which triggers actin polymerization resulting in an elongated shmoo-like morphology[23-25] (Fig. 4A). We thus compared oriented polarization of wild type and *far1-H7* mutant cells, which express a truncated Far1 protein unable to interact with Cdc24 and are unable to orient towards the gradient[26] (Fig. 4B). Specifically, we quantified the angle between the major cell axis and the applied α-factor gradient (0-200 nM) (Fig. 3D and 4C). At lower concentrations (for example, 0 – 60 nM in Fig.4C), the majority of wild-type cells oriented towards the higher concentrations of α-factor. In contrast, *far1-H7* mutant cells responded to the α-factor gradient but randomly oriented their shmoos (Fig. 4C). We noted a slight tendency of the elongating cells to align with the flow, most likely because shmooing cells have a reduced surface that touches the concanavalin A-coated glass and thus become more sensitive to flow-induced distortion. We scored a polarization angle (θ) between $-60^\circ < \theta < 60^\circ$ as "*aligned*", $60^\circ < \theta < 120^\circ$ or $-120^\circ < \theta < -60^\circ$ as "*between*", and $-180^\circ < \theta < -120^\circ$ or $120^\circ < \theta < 180^\circ$ as "*unaligned*" (Fig. 3D and 4D). More than 50% of wild-type cells were scored as "*aligned*", and less than 20% were "*unaligned*". In contrast, the frequency of cells scored in each category was close to 30% for the *far1-H7* cells (Fig. 4D), confirming that Far1 to Cdc24 interaction is required for sensing the direction of the mating factor gradient.

The method described so far uses morphological changes such as cell elongation to quantify the directional response. However, this method is not suitable to score the early events involved in polarity establishment, which precede the morphological changes requiring new cell wall synthesis, and can thus not easily be scored during the first hour after α-factor addition. To circumvent this limitation, we expanded the Matlab-based image analysis program to include the asymmetric localization of fluorescently tagged polarization markers. For example, Cdc24 is recruited to sites of polarization, and thus serves as a molecular marker for orientated polarization in a mating gradient[27, 28]. To visualize Cdc24 by quantitative live cell imaging, we constructed strains harboring at the endogenous locus Cdc24 fused to qV (quadruple Venus, green in Fig. 4E). These strains also express mCherry fused to a transmembrane domain (TMD), which uniformly marks the plasma membrane (red in Fig. 4E). In cells exposed to α-factor gradient, Cdc24-qV is recruited to the membrane and remains at the elongation shmoo tip (Fig. 4E). To quantify membrane-recruitment of Cdc24 in pheromone gradients, we segmented the cell border as "membrane", defined angular elements and measured the intensity of each element. The dynamics of polarized elongation was quantified by measuring the angular distance from the initial centroid (Fig. 4F). At early time points, the cell morphology was nearly circular and thus the angular distance was equal (represented as monotonic color in Fig. 4G). As cells progressively elongated in the direction of the gradient, the angular distance approached 0° (represented as red-like color). However, while the cells only gradually changed their morphology, we observed earlier recruitment of Cdc24 to sites of polarization aligned with the α-factor gradient (Fig. 4H). Moreover, Cdc24 levels at these sites were gradually increased with time. Together, this analysis demonstrates that Cdc24 is recruited and accumulates at sites of polarization in the direction of the gradient and that these dynamic events occur earlier than the morphology changes. Importantly, this method can be used to quantify the spatial and temporal localization of other polarization markers and will also allow for deducing dependencies and temporal order of the downstream events.

Quantitative explanation of random orientation behavior of wild type cell even in α-factor gradient

We next used the established microfluidic assay platform to investigate how the shallow gradient across the yeast cells can be amplified to establish a stable axis of polarity. As a first step, we changed the gradient to determine the range of α-factor concentrations that are compatible with orientation. At lower concentrations (0 - 50nM), the majority (75 %) of wild type cells efficiently aligned along the α-factor gradient (Fig. 5A). In contrast, at higher concentrations (150 - 200nM), the frequency of aligned cells became lower (49.5%), which is possibly explained by the fact that all receptors are bound to pheromone under these conditions. We postulated that the difference in bound receptors in the front and rear of the cell (Fig. 5B) was considered as an approximate amount of signal required to trigger oriented polarization. To estimate the number of bound receptors on each side of the cell, we assume that the receptor density is uniform over the entire cell surface, which is experimentally supported at least at the beginning of the process[29]. The number of bound receptors is calculated as $N \times C / (C + K_d)$, where N is the total number of receptors, C is the concentration deduced from the concentration gradient profile and K_d is the equilibrium dissociation constant of the receptor. The total number of bound receptors for the hemispheres facing (front) and away (rear) in the gradient were calculated by integration over the angles 0 to 180 degree and 180 to 360 degree, respectively, using the integral of the equation: $N \times C / (C + K_d)$. Interestingly, this model predicts that the number of bound receptors on both sides will increase with increasing concentrations, but the difference between the two sides decreases tremendously at higher concentrations. The occupancy difference is predicted to be significantly larger at lower concentrations (0 – 50 nM), even though the absolute concentration is lower. These simple calculations are consistent with the quantitative measurements shown in Fig. 5A, and thus help to understand how the small difference in receptor occupancy is sufficient to accurately orient cell growth towards the gradient source. Additional mechanism may further enhance the difference in receptor

occupancy in pheromone gradients, including α-factor dependent receptor upregulation[30], and polarized secretion.

Summary and Perspective

Here, we developed a quantitative and dynamic assay platform for single cell chemotaxis and characterized the temporal and spatial regulation of polarization in a morphogenetic gradient. Specifically, we combined a computer-controlled microfluidic device with subcellular microscopic imaging and automated image analysis. This assay platform can produce robust and accurate gradient profiles, which successfully mimics the conditions required for the directional polarization of budding yeast cells in pheromone gradients. We validated this versatile assay platform by quantitatively comparing the polarized signaling response of wild-type and orientation-deficient *far1-H7* mutant cells. Moreover, we applied a simple mathematical model to probe whether the difference in receptor-occupancy across yeast cells is sufficient to explain polarized orientation in different gradients. The results show that our integrated assay platform for single cell chemotaxis is able to produce quantitative data sets, which serve as a basis to verify and improve mathematical models of this dynamic process.

We envision that our experimental and analysis platform will allow to design experiments to identify the molecular regulatory mechanisms underlying establishment of cellular orientation in a morphogenetic gradient. While the main protein components of the polarization pathways such as Far1 and Cdc24 are known, the regulatory mechanism by which these proteins are asymmetrically localized within the cell to initiate a directed response remains unclear. There is limited understanding of how an unpolarized cell breaks its symmetry and then amplifies a small initial biochemical activity difference into a stable morphological response towards the gradient by positive and negative feedback. Interestingly, Cdc24-binding deficient mutants of Far1 such as *far1-H7* can, however, still

polarize towards the incipient bud site, resulting in delayed shmoo formation and random orientation in the gradient, which severely decreases mating efficiency. Currently, we speculate that the Far1 RING domain might be required for full activation of Cdc24 and the polarity machinery, and that it may integrate a positive and negative phosphorylation feedback loops analogous to the active role of the Ste5 scaffold protein in MAPK signaling. We expect that knowledge of the spatial and temporal localization of Cdc24 may provide important insight whether and how these feedback mechanisms are regulated by phosphorylation.

Importantly, this integrated platform is versatile, providing greater flexible and opportunity for improvement in comparison with gravity-driven flow or syringe pumps. Additional options can be implemented and computer-controlled, including altering the gradient steepness, switching of the gradient direction, or addition of specific inhibitors at any given time. For example, the current design could achieve 180° switching of the gradient direction by adding additional inlets in the upper and lower parts of cell culture chamber. Additionally, the current design could be improved by controlling the angle of the gradient direction switching (e.g. 90° rotated gradient) to allow to study the molecular mechanisms how cells correct and continuously adjust their polarity. Such perturbations are particularly important to investigate the dynamic cellular feedback and control mechanisms governing chemotaxis, and in particular to probe the plasticity of polarization signaling. Finally, the experimental platform can easily be adapted to investigate chemotaxis in higher eukaryotes, and may thus have wide applications to elucidate the underlying mechanisms of cancer metastasis and inflammatory diseases.

Experimental

Microfluidic device

The microfluidic device was made with polydimethylsiloxane (PDMS, Sylgard 184, Dow Corning) mold by soft lithography. It was fabricated (height = 40 μm) using negative photoresists (SU-8 2050 or SU-8 50, Microchem Corp.). PDMS base and curing agent (10:1 ratio) were thoroughly mixed, degassed in a vacuum chamber, and then poured on the mold, and cured on hot plate (65°C in 1 hr and 130°C in 30 min). The cured PDMS was then carefully peeled off the mold. The inlet and outlet holes were punched by a flat-tip. Both a glass slide and the PDMS structures were treated with UV Ozone cleaner (PSD-UVT, Novascan) for 6 min to bond together. Feeder wells (bottomless well-strip, Evergreen) were glued on the PDMS chips. The reservoirs were connected with gas-tight rubber and tube. By compressed air pressure onto medium in reservoir, the medium with or without α-factor was introduced, and concentration gradient of α-factor was generated in the cell culture chamber (Fig. 2A and Supplementary Fig.S2 and S3). The compressed airflow was provided by the diaphragm pump, the compressed air tank, the electronic pressure regulator, and solenoid valves (ONIX, CellASIC Corp). We note that the system was assembled by different combinations of components[31] and the proper range of pressure should be chosen in consideration of fluidic Ohm's Law and microfluidic chip design. The profiles such as pressure and time were programmed into the software and executed during imaging.

Yeast preparation

Budding yeast cells were grown overnight to saturation and then allowed to resume exponential growth by diluting them 50-fold into fresh growth medium (Synthetic Defined Media with 2% glucose, OD_{600} ~ 0.1), and incubating them for ~ 3 hours at 30°C before the experiment. They were mildly sonicated for 1 min, and introduced into the microfluidic

chamber. A micropipette tip with the cell suspension was inserted in the cell inlet hole to introduce (20-100 μL) to microfluidic cell culture chamber by gravity flow. After sufficient loading, the tip was carefully removed and the cells in the microfluidic chamber were incubated for 30 minutes. The yeast α-factor was purchased from Genscript. The genotype of the strain is described in Supplementary Table S1.

Live cell imaging

For attaching yeast cells on the glass of PDMS device, concanavalin A (GE Healthcare) in phosphate-buffered saline (PBS: 1 mg/ml) was flowed and coated on the glass during 10-30 min. The microfluidic chamber was rinsed with cell culture medium before loading the cells. The gradient of α-factor concentration was visualized by addition of fluorescent dye (tetramethylrhodamine-dextran, Invitrogen; or Dextran-Alexa 680, *M.W.*=3000, invitrogen). We assumed the concentration profile of the dye is similar to α-factor's. The microfluidic device was mounted on the stage of an inverted microscope (Eclipse Ti, Nikon Instruments). Images of yeast cells in the device were acquired on fully automated inverted fluorescence microscope in a temperature incubator set at 30°C, with appropriate excitation and emission filters.

Image analysis and data extraction

Image analysis was conducted using a Matlab script. The analysis of the yeast polarization dynamics consists of three major steps. First, we applied a pre-processing step to stabilize alignment problems caused by the instabilities of the microscope stage, if it was required. We observed instability of the microscope stage as flickering in the time-lapse images, and developed an automated correction step to align the images in the movie. These stage problems appear as a translation on the x and y axes, and rotation was not

observed. To correct, we analyzed the strongest cross-correlation between the subsequent frames:

$$(f_t \bullet f_{t+1})[n] = \sum_{m=-\infty}^{\infty} f_t^*[n] f_{t+1}[n+m],$$

where f_i denotes the i^{th} frame, and asterisk refers the complex conjugate operator. Since calculating cross-correlation in the image space is computationally intensive, we calculated it in the Fourier-domain, where it becomes a point-wise multiplication of the complex conjugate of f_t and f_{t+1}.

Second, we segmented the outline of the cell using an active contour model, so called gradient vector flow (Note: here, "gradient" is not referring to the α-factor concentration gradient but to the intensity gradient of the cell object image). In order to accurately detect the outline of the cell - the biggest and most challenging part of the data analysis - we used active contours[21] extended with the gradient vector flow[22] framework. Contours were manually initialized on the first frame or on their first appearance, and contour evolution was preformed till convergence. On subsequent frames initial contours were derived from previous steady states and evolved. The external (*i.e.* calculated from the grayscale image) energy was designed such that it drives the contour towards high intensities, in our case - towards the inner side of the cell. To perform the segmentation, a Matlab program was designed with graphical user interface. This allows user to load and browse image sequences, manually add, delete, evolve, and propagate contours, track them over time and calculate statistics.

Finally, we tracked contours over time, and extracted morphological and intensity-based features – cells and membrane - to quantitatively describe the dynamics of intracellular polarization or cell morphology. The two main steps of post processing are the tracking of the contours and calculating their spatial and temporal features. Based on the center of mass of the detected cell outline, the IDL tacking algorithm[32] was applied. The final

statistics was calculated in two different levels, and first properties of each individual cell outlier (membrane) were determined. Thus, we calculated dynamics of cell morphology (*e.g.* circularity, perimeter, length with angle toward gradient direction) and dynamics of intracellular behavior (*e.g.* gene expression of mating pathway, localization of CDC24 with angle information toward gradient direction). Properties of individual tracks were determined on basis of the above features, and temporal behavior was analyzed.

Acknowledgments

This work was supported by the Competence Center for Systems Physiology and Metabolic Diseases (CC-SPMD), the Swiss Initiative in Systems Biology (SystemsX.ch), the European Research council (ERC) and the ETHZ. The authors would like to thank the staff in FIRST-CLA, the Department of Biosystems and Science Engineering (D-BSSE) for initial support of the project, and Anton Lehmann for helping to build the experimental platform. We are grateful to Dr. Alicia Smith for editing this manuscript, and members of the Peter lab for critical feedback and helpful discussions.

References

1. D. Muzzey and A. van Oudenaarden, *Annu Rev Cell Dev Biol*, 2009, **25**, 301-327.
2. A. R. Kherlopian, T. Song, Q. Duan, M. A. Neimark, M. J. Po, J. K. Gohagan and A. F. Laine, *BMC Syst Biol*, 2008, **2**, 74.
3. S. G. Megason and S. E. Fraser, *Cell*, 2007, **130**, 784-795.
4. Y. Sako, *Mol Syst Biol*, 2006, **2**, 56.
5. M. R. Bennett and J. Hasty, *Nature Reviews Genetics*, 2009, **10**, 628-638.
6. M. R. Bennett, W. L. Pang, N. A. Ostroff, B. L. Baumgartner, S. Nayak, L. S. Tsimring and J. Hasty, *Nature*, 2008, **454**, 1119-1122.
7. D. N. Breslauer, P. J. Lee and L. P. Lee, *Mol Biosyst*, 2006, **2**, 97-112.
8. P. Hersen, M. N. McClean, L. Mahadevan and S. Ramanathan, *Proceedings of the National Academy of Sciences of the United States of America*, 2008, **105**, 7165-7170.
9. S. Pelet, F. Rudolf, M. Nadal-Ribelles, E. de Nadal, F. Posas and M. Peter, *Science*, 2011, **332**, 732-735.
10. M. TessierLavigne and C. S. Goodman, *Science*, 1996, **274**, 1123-1133.
11. J. F. Cote and K. Vuori, *Science*, 2009, **324**, 346-347.
12. P. Friedl and K. Wolf, *Nature Reviews Cancer*, 2003, **3**, 362-374.
13. J. E. Segall, *Proceedings of the National Academy of Sciences of the United States of America*, 1993, **90**, 8332-8336.
14. L. G. Vallier, J. E. Segall and M. Snyder, *Cell Motility and the Cytoskeleton*, 2002, **53**, 251-266.
15. T. I. Moore, C. S. Chou, Q. Nie, N. L. Jeon and T. M. Yi, *Plos One*, 2008, **3**, e3865.
16. S. Paliwal, P. A. Iglesias, K. Campbell, Z. Hilioti, A. Groisman and A. Levchenko, *Nature*, 2007, **446**, 46-51.
17. A. Liebmann-Vinson, in *ACS Symposium Series*, American Chemical Society, 1999, pp. 474-494.

18. D. Nychka, G. Gray, P. Haaland, D. Martin and M. OConnell, *Journal of the American Statistical Association*, 1995, **90**, 1171-1178.

19. M. C. Gustin, J. Albertyn, M. Alexander and K. Davenport, *Microbiology and Molecular Biology Reviews*, 1998, **62**, 1264-1300.

20. K. Johanson, P. L. Allen, R. A. Gonzalez-Villalobos, C. B. Baker, R. D'Elia and T. G. Hammond, *Biotechnology and Bioengineering*, 2006, **93**, 1050-1059.

21. M. Kass, A. Witkin and D. Terzopoulos, *International Journal of Computer Vision*, 1987, **1**, 321-331.

22. C. Y. Xu and J. L. Prince, *1997 IEEE Computer Society Conference on Computer Vision and Pattern Recognition, Proceedings*, 1997, 66-71

23. A. C. Butty, P. M. Pryciak, L. S. Huang, I. Herskowitz and M. Peter, *Science*, 1998, **282**, 1511-1516.

24. Y. Shimada, M. P. Gulli and M. Peter, *Nature Cell Biology*, 2000, **2**, 117-124.

25. N. Valtz, M. Peter and I. Herskowitz, *Journal of Cell Biology*, 1995, **131**, 863-873.

26. J. Chenevert, *Molecular Biology of the Cell*, 1994, **5**, 1169-1175.

27. A. Nern and R. A. Arkowitz, *Journal of Cell Biology*, 1999, **144**, 1187-1202.

28. K. A. Toenjes, M. M. Sawyer and D. I. Johnson, *Current Biology*, 1999, **9**, 1183-1186.

29. K. R. Ayscough and D. G. Drubin, *Current Biology*, 1998, **8**, 927-930.

30. C. Davis, P. Dube and J. B. Konopka, *Genetics*, 1998, **148**, 625-635.

31. K. W. Bong, S. C. Chapin, D. C. Pregibon, D. Baah, T. M. Floyd-Smith and P. S. Doyle, *Labchip*, 2010, **11**, 743-747.

32. J. C. Crocker and D. G. Grier, *Journal of Colloid and Interface Science*, 1996, **179**, 298-310.

Figure legends

Fig. 1: Quantitative assay of single cell chemotaxis (A) Schematic illustration of the budding yeast polarization process in mating. Two haploid yeast of opposite mating types (**a** and **α**) secrete pheromones that bind to dedicated receptors expressed on **a**- or α-cells respectively (left). Activated receptors initiate a signaling pathway triggering cell cycle arrest and formation of a polarized projection (shmoo) (right), which ultimately culminates in the formation of **a**/α diploid cells **(B)** Overview of the microfluidic device used to generate morphogenetic gradients (α-factor concentration) across the cell culture chamber**.** The gradient is established between the high and low concentration channel by diffusion. An array of micropillar near the cell culture chamber reduces the flow-induced perturbation on cell orientation. **(C)** Yeast polarization in the microfluidic device, a yeast cell elongates toward higher concentration of α–factor, whose gradient was generated by the microfluidic device. In this process, Cdc24 asymmetrically localizes at the membrane, and accumulates at sites oriented towards the higher concentration of α-factor. Cdc24 fused to yellow fluorescent protein (quadruple Venus) was visualized by live cell microscopy (green). These strains also express mCherry fused to a transmembrane domain (TMD), which uniformly marks the plasma membrane (red). **(D)** Schematic illustration of yeast polarization quantification. Images of single yeast cells were segmented, and their morphological polarization axis was quantified. The polarization axis was defined by measuring the angle between the growth axis and the gradient direction (left). To create a data set, the polarization axis of a set of cells was mapped to a circle in which 0° represents perfect orientation towards the gradient. Each cell is represented by a dot, and the radius indicates the diffusible factor concentration based on the position of the cell relative to the gradient. The resulting data sets serve as a basis to compare the polarity of strains.

Fig. 2: Design principles of the microfluidic device and regulation and stability of the generated gradients. (A) Overview of the microfluidic set-up used to generate morphogenetic gradients. The gradient is established by diffusion of a diffusible substance (e.g. α-factor) across the cell culture chamber. There are two liquid feeder wells, which may contain varying concentrations of the diffusible substance. Liquid in the feeder wells is delivered to the cell culture chamber by compressed air pressure (ΔP_H, ΔP_L). Importantly, the gradient profile can be tuned by controlling the ratio of the pressures (e.g. $\Delta P_H / \Delta P_L$). The fluidic resistances near to solution reservoirs are designed to tune the flow rate and external fluctuation when we apply pressure (ΔP) to the reservoirs. **(B)** Simulation of flow velocity in microfluidic cell culture chambers. An array of micropillars near the cell culture chamber reduces the flow-induced perturbation of cells. Arrows indicate the direction of the flow and the flow velocity in the cell culture chamber is lower (dark blue) than that above and below the micropillars. The simulation results presented are for inlet mean velocity **=** 1 mm/s. **(C) and (D)** Compressed air pressure ($\Delta P_H = \Delta P_L = 3$ *psi*) was continuously provided to the solution reservoirs in order to establish the gradient profiles **(C)**, which were visualized by the fluorescent dye (tetramethylrhodamine-dextran) at the times indicated (min). **(D)** The intensities between the upper and lower barrier were quantified by fluorescence microscopy. **(E)** The stability of the established gradients was controlled at the times indicated. **(F) and (G)** The gradient profile was regulated by changing the magnitude of the input pressure on the reservoirs containing two concentrations of tetramethylrhodamine-dextran. The concentration **(F)** and intensity **(G)** of the gradients at the indicated pressure ratio was quantified by fluorescence microscopy as described above.

Fig. 3: Quantitative single cell analysis of yeast polarization in space and time. (A) Time-lapse imaging of yeast cells exposed to a concentration gradient of α-factor. The cells express a fluorescent protein reporter (green) under the control of the *FIG1*-promoter, which

is specifically induced by α-factor. Note that the cells directionally polarize towards the higher α-factor concentration (blue, upper side). Cells (marked by arrowhead) can adjust their angle of polarized growth during the process. **(B) – (D)** Quantification of oriented cell polarization**. (B)** Segmentation. A sub-image (yellow box in Fig.3A) is shown as an example. The cell shape was segmented by active contours. The contours were initialized on the first frame (red line) and contour evolution was preformed till convergence (blue line). Detailed information is provided in the experimental section. The segmentation is used for the quantification of polarization dynamics **(C)** Quantification of cell morphology and intracellular changes upon application of the α-factor gradient. The gradual cell elongation was quantified by measuring the perimeter (top graph) and circularity (middle graph). Expression of the p*FIG1*-qV reporter (yellow fluorescent protein) upon application of the α-factor gradient was quantified by measuring the total YFP intensity in the segmented cell (bottom graph). The graph shows an analysis of 15 cells in Fig.3A. **(D)** The directed polarity response was quantified by plotting the orientation angles of cells 240 min after applying the α-factor gradient. The polarization axis was mapped to a circle in which 0° represents perfect orientation towards the gradient. Each cell in Fig.3 is represented by a dot and the radius indicates the α-factor gradient position in nM concentration.

Fig. 4: Quantitative analysis of wild-type cells and cells lacking a functional mating scaffold Far1. (A) Simplified illustration of the role of Far1 in linking activated pheromone receptors via Gβγ to the intracellular polarization machinery composed of Cdc24, Bem1 and Cdc42. The gradient direction is sensed by bound α-factor receptors, which locally triggers dissociation of the associated heterotrimeric protein. In turn, Gβγ recruits the Far1-complex to the polarization site. (**B**) Schematic illustration of wild-type Far1 and the truncated Far1-H7 mutant protein. The RING-domain of Far1 (grey) mediates its interaction with Gβγ, while Cdc24 binds to the carboxy terminus. Note that this Cdc24 binding domain is lacking in the

Far1-H7 mutant. (**C**) and (**D**) Oriented polarization of wild type (WT) and *far1-H7* cells in a 0-200 nM α-factor gradient was quantified using wheel plots as described in the legend of Fig.3 D. Note that the majority of the wild-type strain aligns along the pheromone gradient, while *far1-H7* cells polarize in a random direction with respect to the gradient. **(D)** The frequency of "aligned", "between" and "unaligned" cells was plotted in a bar diagram. The following criteria were applied: Orientation angle θ, "Aligned" -60° < θ < 60°; "Between" 60°< θ <120° or -120°< θ < -60°; "Unaligned" -180°< θ < -120° or 120°< θ <180°. **(E) – (H)** Polarized localization of Cdc24 in α-factor gradient. **(E)** Cdc24 fused to qV (quadruple Venus) was visualized by live cell microscopy (green). These strains also express mCherry fused to a transmembrane domain (TMD), which uniformly marks the plasma membrane (red). Cdc24 asymmetrically localized at the membrane and accumulated at sites oriented towards the higher concentration of α-factor. **(F)** Illustration of "angular distance" and "angular intensity": The "angular distance" is defined by the length from initial centroid of the segmented cells to cell membrane in given angle β. The "angular intensity" is defined by the intensity of Cdc24 at the membrane in given angle β **(G)** The dynamics of polarized cell elongation was quantified by "angular distance" **(H)** The dynamics of Cdc24 localization is quantified by "angular intensity". Note that Cdc24 was recruited and accumulated at sites of polarization determined by the α-factor gradient. Cdc24 recruitment occurred prior to the morphological changes.

Fig. 5: Comparison of experimental data and simulations to describe oriented polarization of yeast cells along α-factor gradients based on asymmetric receptor occupancy. (**A)** Oriented cell polarization was quantified in the indicated α-factor gradient profiles. At a lower concentration range (0 – 50 nM), most cells orient towards higher concentration of α-factor. With increasing concentration range, the portion of directionally polarized (aligned) cells decreases significantly **(B)** Schematic illustration of a yeast cell

exposed to a α-factor gradient. Receptors located in the front portion of the cell can more often engage α-factor. **(C)** Calculating the numbers of bound α-factor molecules in an α-factor concentration gradient. The number of engaged α-factor receptors differs between the front and rear of the cell and was calculated for different gradient profiles. Note that the difference strongly decreases with increasing α-factor concentrations, which is in good agreement with the experimental measurements shown in panel (A).

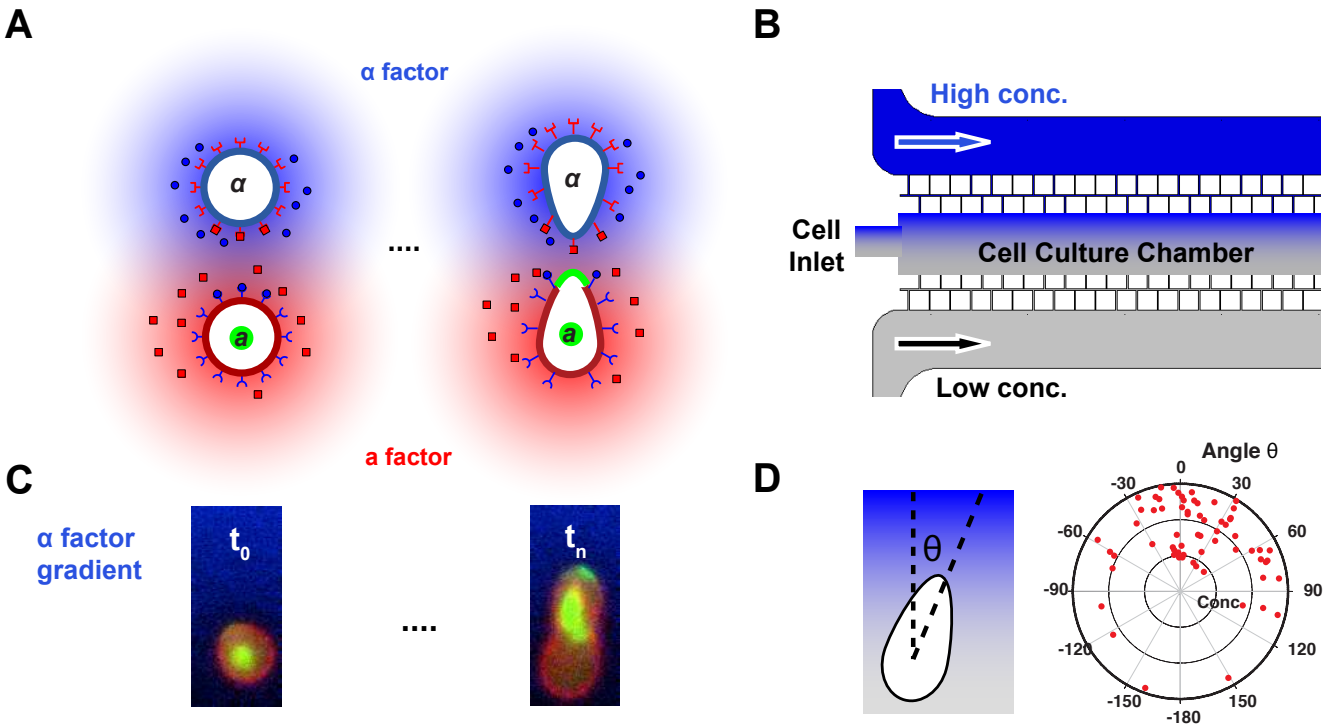

Figure 1 Lee et al

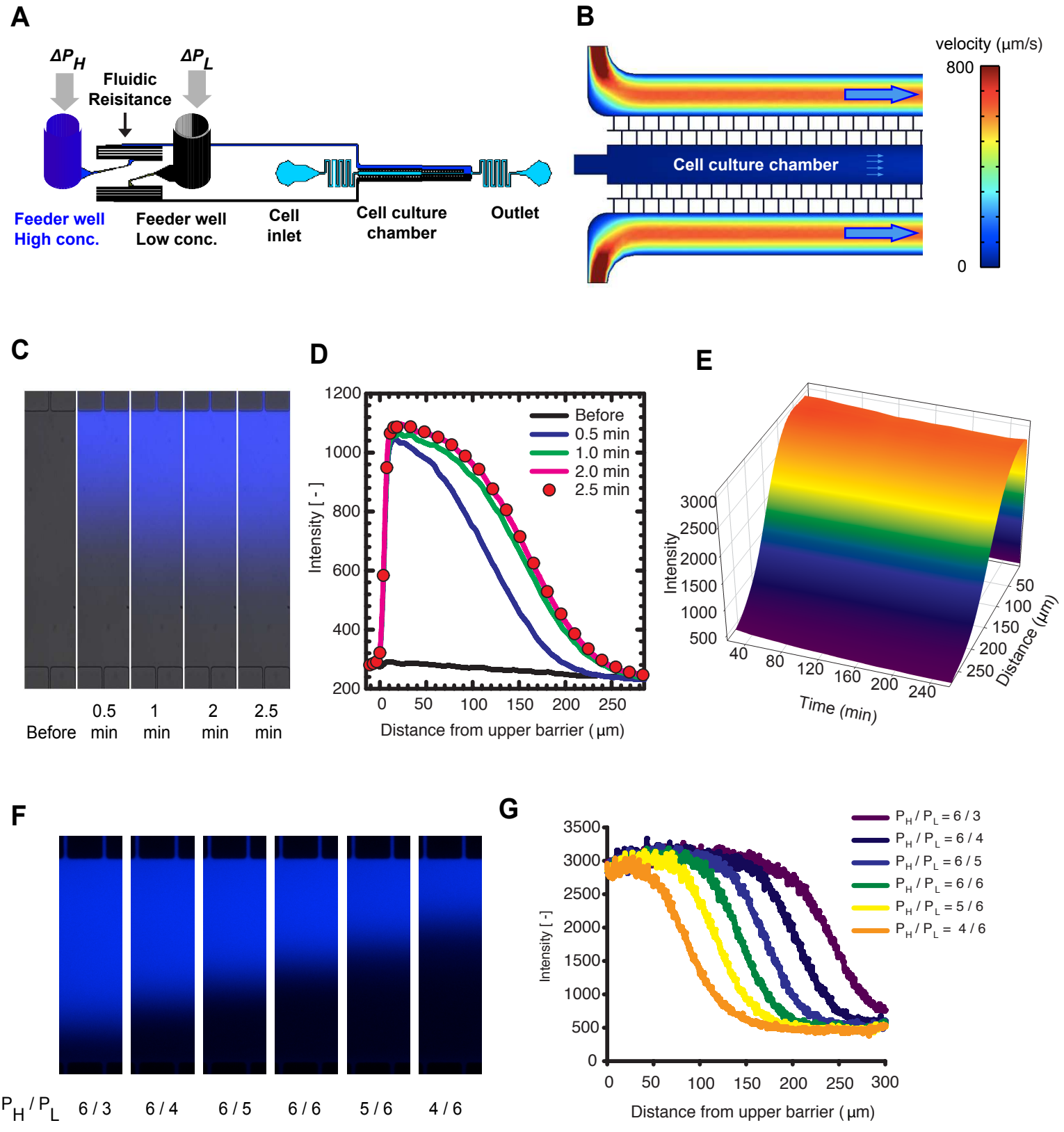

Figure 2 Lee et al.

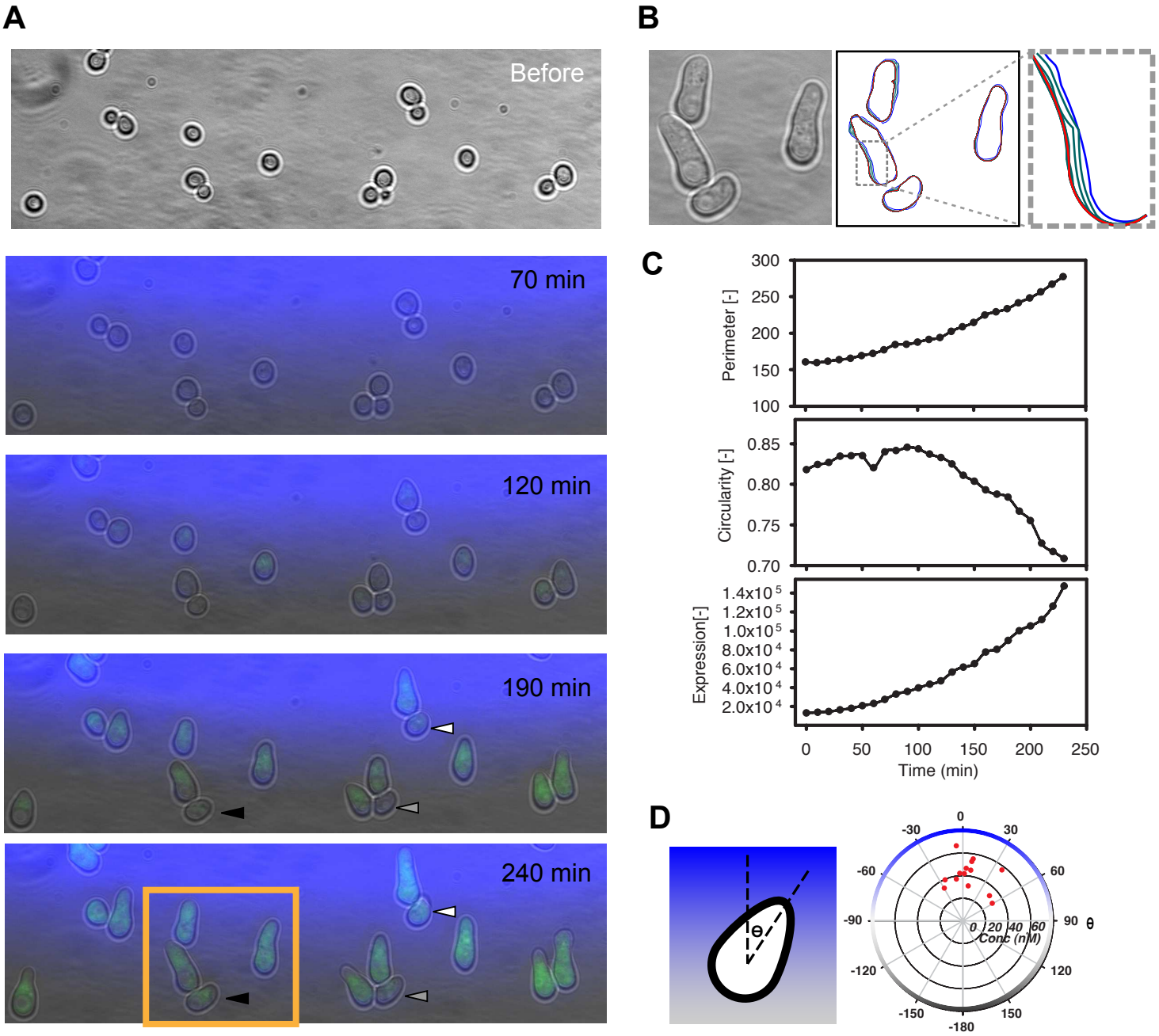

Figure 3 Lee et al.

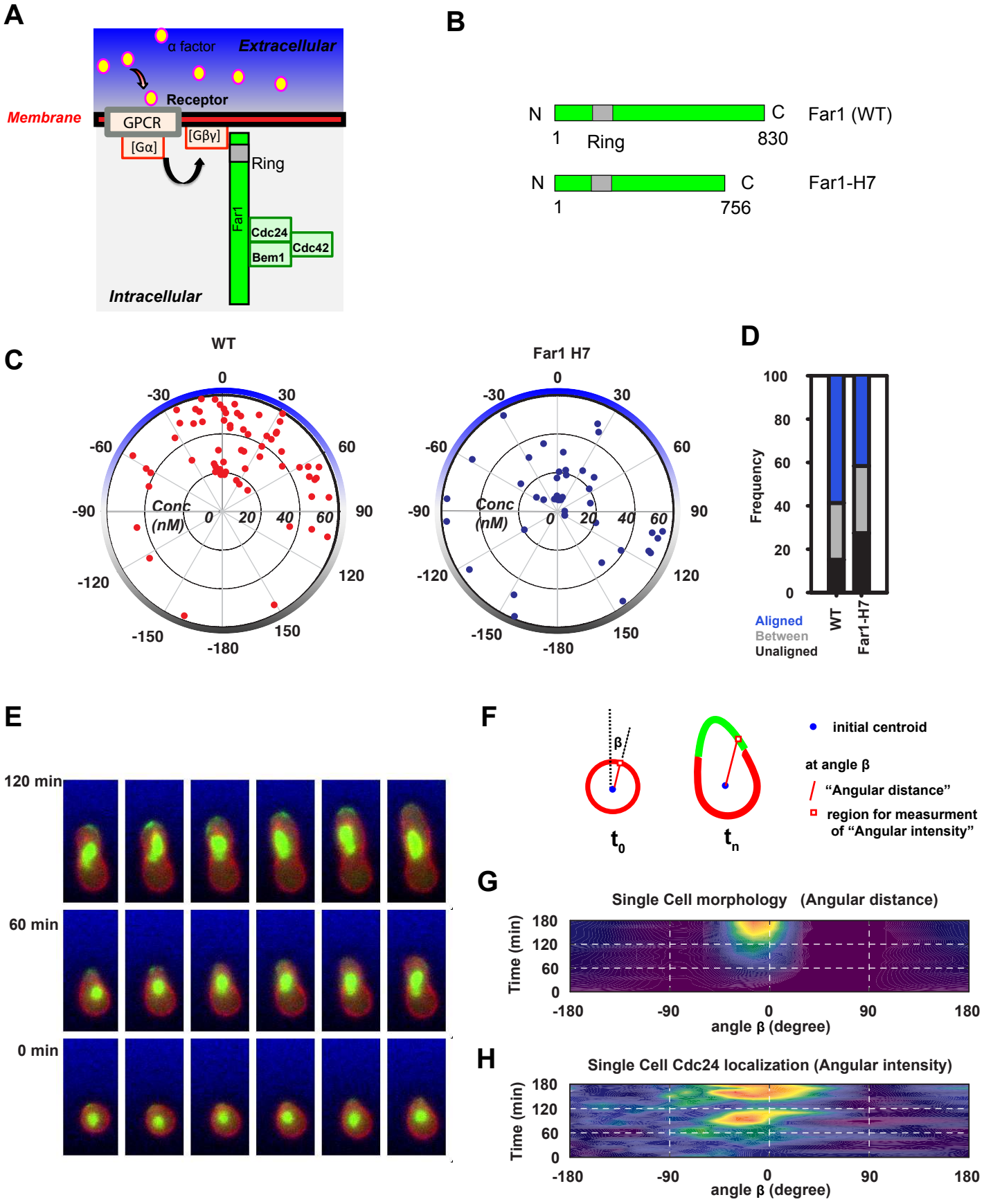

Figure 4 Lee et al.

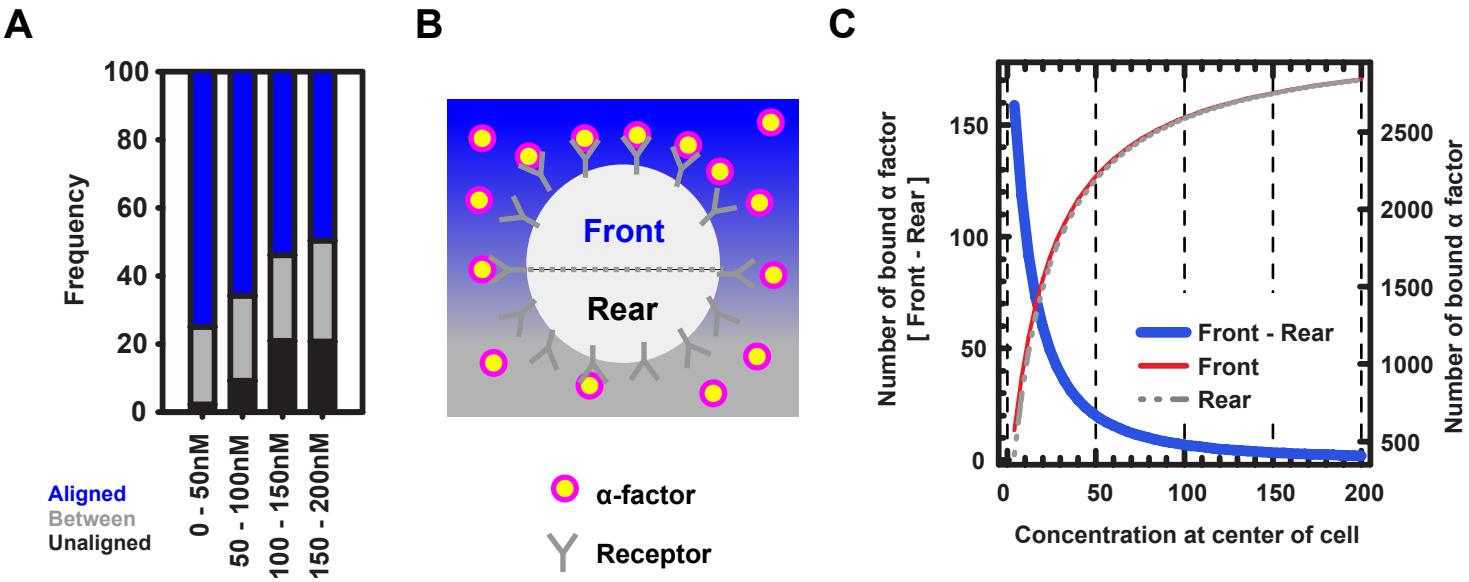

Figure 5 Lee et al.

Supplementary Information:

Quantitative and Dynamic Assay of Single Cell Chemotaxis

Sung Sik Lee [a,b], Peter Horvath [c], Serge Pelet [a,b], Björn Hegemann [a],

Luke P. Lee *,[d], and Matthias Peter §,[a,b]

[a] Institute of Biochemistry, ETH Zurich, Zurich, CH 8093, Switzerland

[b] Competence Center for Systems Physiology and Metabolic Disease(CC-SPMD), Zurich, CH 8093, Switzerland

[c] Light Microscopy Center (LMC), Department of Biology, ETH Zurich, Zurich, CH 8093, Switzerland

[d] Berkeley Sensor & Actuator Center, Department of Bioengineering, University of California, Berkeley, CA 94720-1762, United States

Co-correspondences:

* lplee@berkeley.edu; Tel: +1-510-642-5855, Fax: +1-510-642-5835

§ matthias.peter@bc.biol.ethz.ch ; Tel: +41-44-633-6586, Fax: +41-44-633-1298

Conventional method

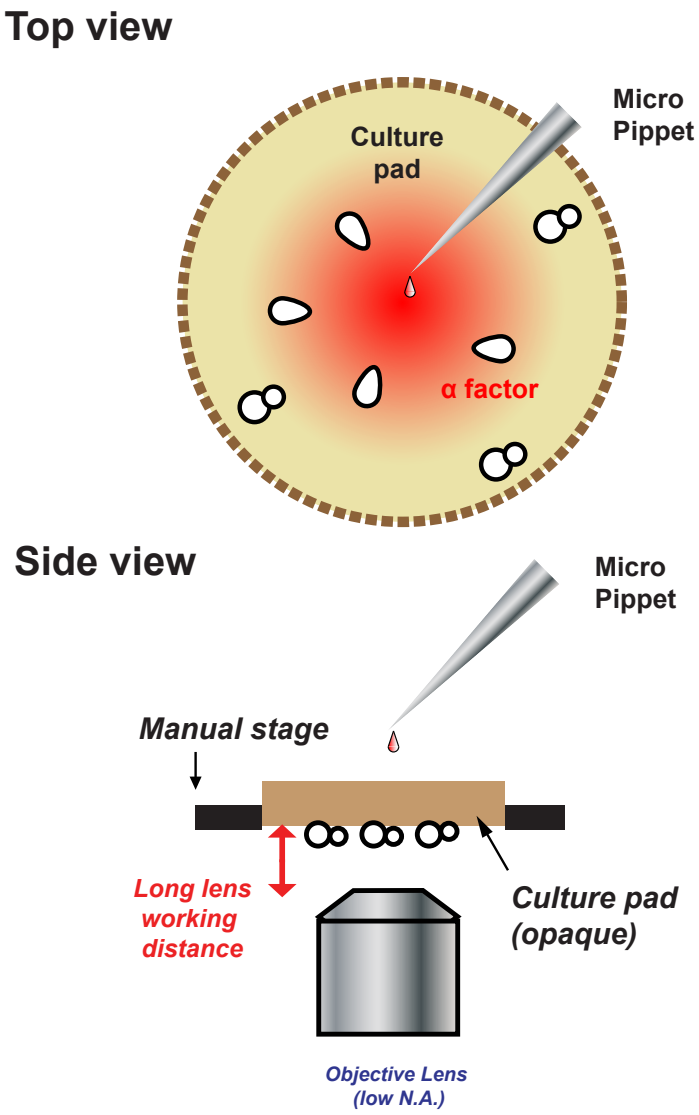

Figure S1: Conventional method for creating an α-factor gradient. α-factor (red drop) solution is continuously dropped on the agarose cell culture pad. This method is limited from high resolution fluorescent imaging because the thick and opaque cell culture pad interferes with fluorescent light and a long-working distance objective lens is needed.

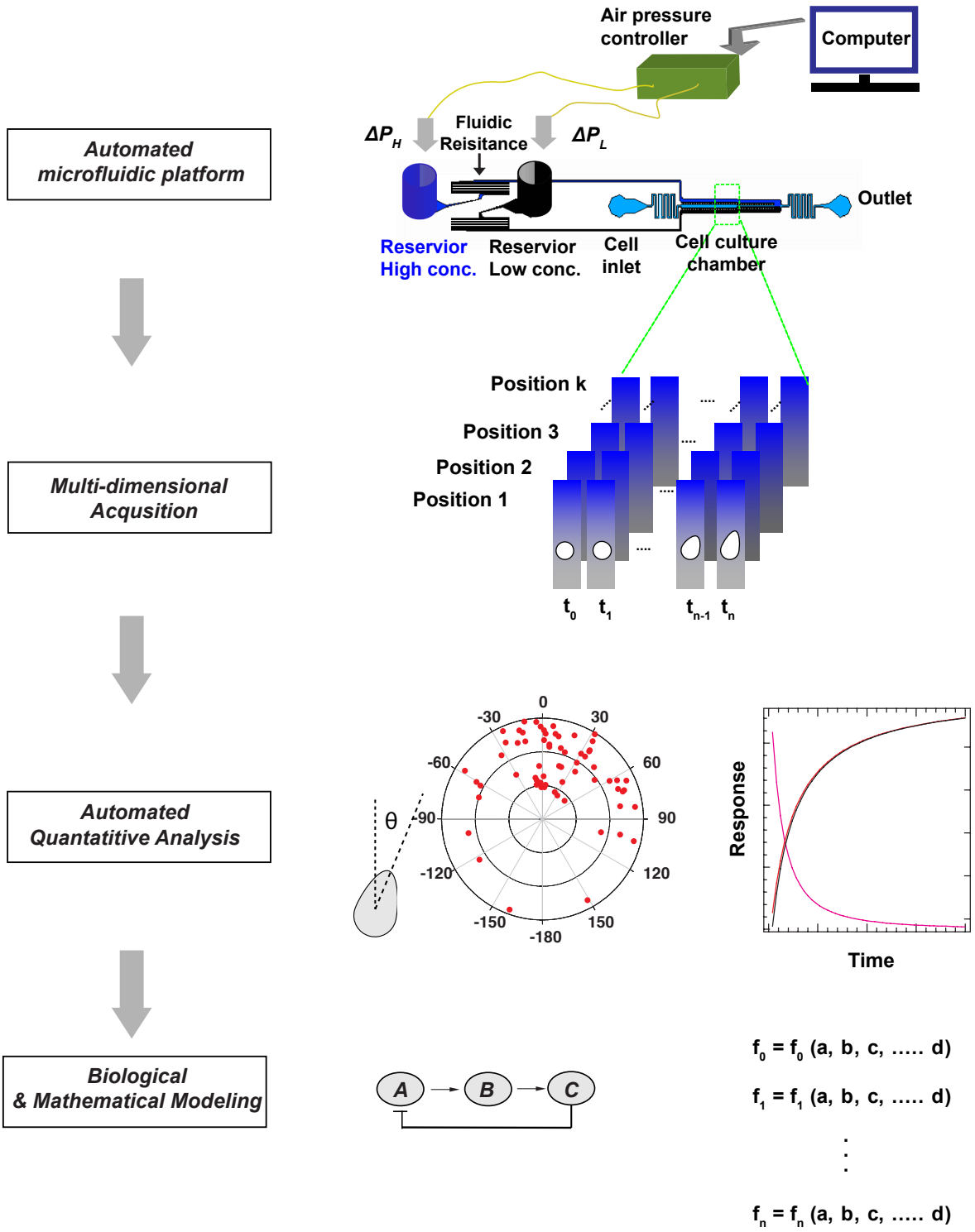

Figure S2: **Integrated platform for quantitative and dynamic assay of single cell chemotaxis.** The automated microfluidic platform can regulate a morphogenetic gradient. By a triggering signal from the computer to the air pressure controller at any given time, high and low concentrations of α-factor are equally provided to the cell culture chamber. Thus, the gradient is established by diffusion of high and low α-factor concentration. The fluidic resistances near the solution reservoirs are designed to tune the flow rate and external fluctuation when air pressure (ΔP) is applied to the reservoirs. The dynamics of budding yeast polarization are multi-dimensionally recorded including positions, fluorescent channels and time. Images of single yeast cells are segmented, and their morphology and subcellular polarization are quantified. The resulting data sets serve as a basis to validate and improve mathematical models describing this dynamic process.

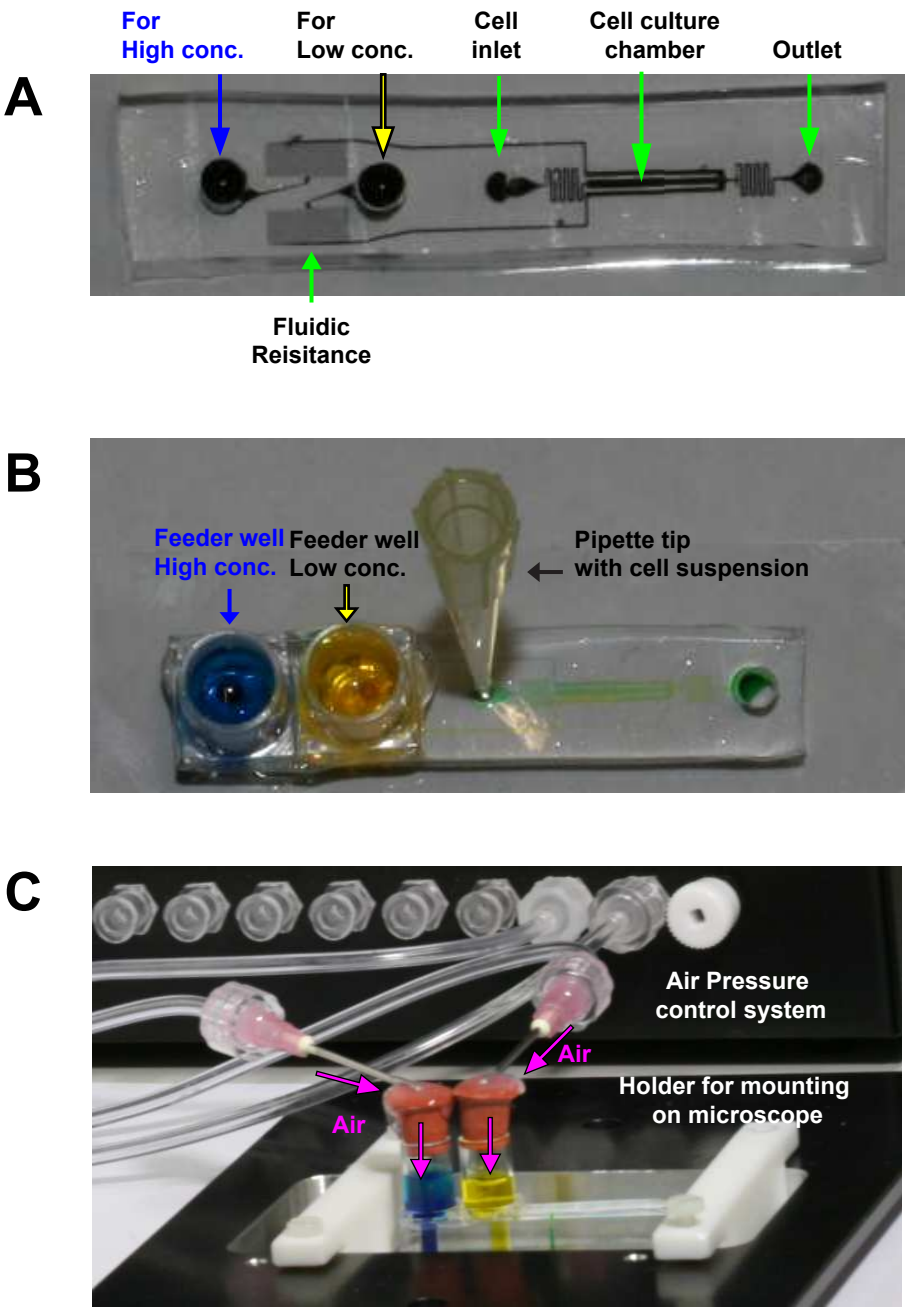

Figure S3: Microfluidic chip and assembly. Overview of the microfluidc chip design (A) Microfluidic chip with feeder wells and pipette tip for cell loading. (B) There are two liquid feeder wells, which may contain varying concentrations of the diffusible substance. A micropipette tip was inserted in the cell inlet hole to introduce (20-100 µL) of the cell suspension to the microfluidic cell culture chamber by gravity flow. After loading, the tip was carefully removed and the cells in microfluidic chamber were examined. (C) Assembly of set-up: the compressed airflow was established by the diaphragm pump, the compressed airtank, the electronic pressure regulator, and the solenoid valves. The airflow was delivered to tow liquid feeder wells.

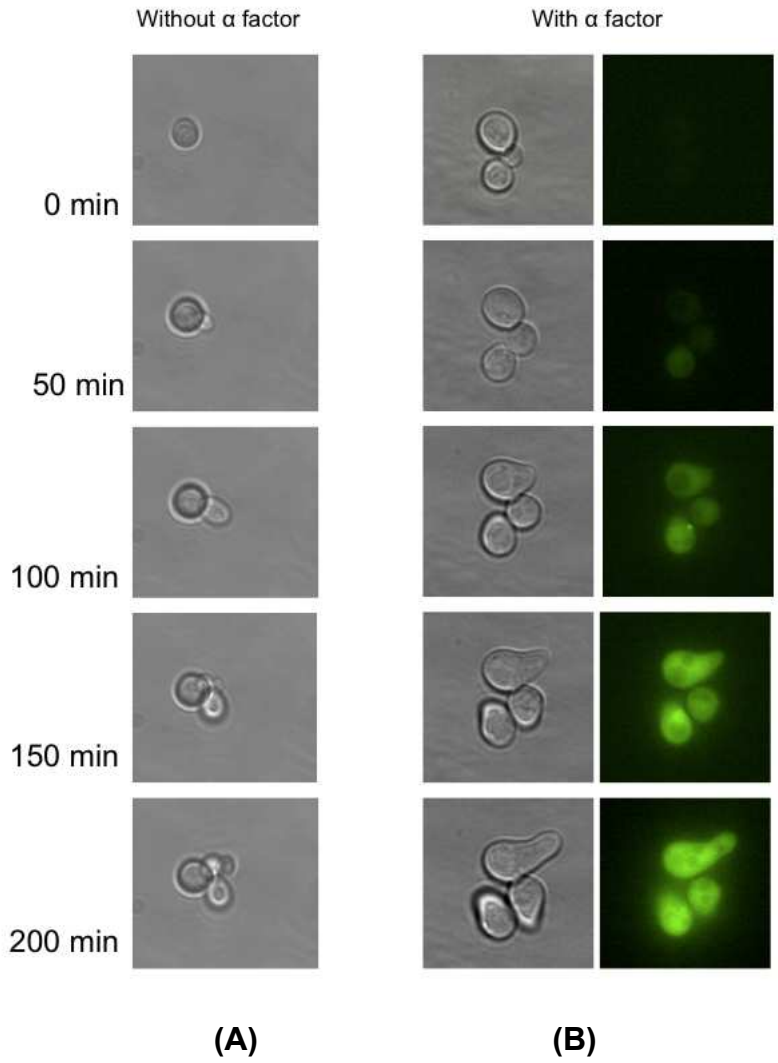

Figure S4: Time-lapse images of yeast cells. Cells grow and continuously make buds without α-factor (A; budding). With uniform α-factor, cells form elongated shapes termed shmoos (B; shmooing). The direction of shmooing is random since α-factor is uniformly distributed and thus binds receptors over the entire cell surface with the same probability. Cells were engineered to express a mating-specific reporter, based on the *FIG1* promoter driving the expression of quadruple-Venus fluorescent protein (*pFIG1*-qV). In response to α-factor, the cells thus express YFP (green), implying that the yeast cells are able to grow and efficiently respond to pheromones in the cell culture chamber for extended periods of time.

Supplementary Table S1: Yeast strains used in this study.

Strain No	Relevant genotype	Reference
EG123	*HMLa HMRa; met ade, ura;*	*Valtz et al., 1995*
ySP107	*EG123 pFIG1-quadVenus::LEU2*	*this study*
yMP315	*EG123 far1-s (H7)*	*Valtz et al., 1995*
BY4741	*MATa ura3Δ0; leu2Δ0; his3Δ1; met15Δ0*	*Openbiosystems*
yBH200	*BY4741 CDC24::CDC24-quadVenus; FAR1::FAR1-HA-2xStrp-G861A-HIS3; pRPS2-TMDmCherry::LEU2*	*this study*

Supplementary Movie S1

Dynamics of yeast polarization under in the microfluidic device in response to an α-factor gradient

The yeast cells polarize towards higher concentrations of mating pheromone (α-factor; blue). The cells express quadruple-Venus fluorescent protein under the control of the mating-specific *FIG1* promoter (green).

Reference

N. Valtz, M. Peter and I. Herskowitz, *Journal of Cell Biology*, 1995, **131**, 863-873.